

# Theoretical Analysis of Diffused Quantum-Well Lasers and Optical Amplifiers

Wallace C. H. Choy and K. S. Chan

*Invited Paper*

**Abstract**—Diffused quantum-well (QW) distributed feedback (DFB) lasers and optical amplifiers will be theoretically analyzed in this paper. For DFB lasers, a design rule will be proposed and the validity of the design rule will be discussed with respect to changes in the injected carrier density. The range of grating period, which can be used in the design, is discussed. As a consequence, the maximum tuning range of the emission wavelength can be estimated without involving the time-consuming self-consistent simulation. The features of polarization independence of optical amplifiers achieved by using diffused QWs are also discussed. Our theoretical results successfully explain why polarization independence can achieve in the long-wavelength tail of the modal gain and absorption coefficient but not at photon energies above the transition edge. This explanation applies to other tensile-strained QWs for polarization-independent applications. The understanding is crucial for optimizing polarization-independent devices. To conclude, our analysis of the diffused QW optical devices demonstrates that QW intermixing technology is a practical candidate for not only realizing monolithic photonic integrated circuit, but also enhancing optical device performance.

**Index Terms**—Diffused quantum well (DFQW), distributed feedback (DFB) lasers, optical amplifiers, polarization independence, quantum-well interdiffusion, quantum-well intermixing, wavelength tuning.

## I. INTRODUCTION

SINCE the first report of disordering of superlattice in 1981 [1], quantum-well (QW) intermixing has been intensely investigated not only for the realization of monolithic integrated optoelectronic circuit [2], but also for improving the performance of optical components such as lasers [3], amplifiers [4], modulators [5], and photodetectors [6]. This is because relatively simple and mature post-growth techniques such as rapid thermal annealing [2] and high-power laser photoabsorption [7] are involved in QW intermixing, which provide useful and controllable changes of optical properties and operation wavelength through the modification of the composition profile. During the interdiffusion of a square QW, atoms in

the barrier QW diffuse into the wells while those in the well diffuse into the barrier. Therefore, the QW potential profile becomes graded and the well bottom will move upward. As a consequence, the optical properties and bandgap energy can be modified for performance enhancement in optical devices. By selectively intermixing different regions of a wafer, monolithic integration of optoelectronic circuits can be achieved. It should be noted that QW intermixing can also be enhanced by introducing vacancies, defects, or dopants with or without charges through, for instance, implantation [8], modification of epitaxy conditions [9], or SiO<sub>2</sub> capping [10].

In the mean time, simulation works have been carried out in diffused quantum well (DFQW) optical devices that play an important role in understanding and optimizing device performance, such as the effects of strain induced by QW intermixing on the band structure and the optical properties of DFQW, in addition to reducing the development cost, which otherwise is very expensive using experimental approaches. The optical properties studied include absorption coefficient [11], [12], gain [13]–[15], and refractive index [16]. In order to study the effects of QW intermixing on material optical properties and, thus, the device performance, DFQW band structure taking into account the modification of material parameters has to be simulated. The material parameters are composition profile, strains, effective mass, and so on. The calculated bandgap energy of DFQW is also a crucial parameter for optimizing the operation wavelength, particularly for those optical devices that are sensitive to the absorption edge such as waveguide-type electroabsorption modulators, photodetectors and passive waveguides. Recently, some interesting Fabry–Perot and distributed feedback (DFB) laser structures using DFQW have been proposed [17], [18], even though there is no experimental demonstration due to the complexity of the proposed structures.

To enhance device performance, QW intermixing has been utilized in different regions of device structures. For instance, DFQWs have been introduced to form window structures at the facets of lasers [3] and photodetectors [6] based on blue-shifting the bandgap energy. As a result, the catastrophic optical damage is diminished and the output power of the laser and the detected power of the photodetector significantly increase. By using DFQW as the active region of the optical devices, it can improve the optical properties such as reducing the polarization sensitivity, which is an inherent feature of QW, and tuning the operation wavelength (to be discussed later in detail).

Manuscript received December 18, 2002; revised June 24, 2003. This work was supported in part by the seed funding of the Hong Kong University Research Grant Council (Account 10203994/24641/14300/301/01), and in part by a grant from City University of Hong Kong (Project 7001460-610).

W. C. H. Choy was with Fujitsu Compound Semiconductor Inc., San Jose, CA 95131 USA. He is now with the Department of Electrical and Electronic Engineering, University of Hong Kong, Hong Kong (e-mail: chchoy@eee.hku.hk).

K. S. Chan is with Department of Physics and Materials Science, City University of Hong Kong, Kowloon, Hong Kong.

Digital Object Identifier 10.1109/JSTQE.2003.818842

In this paper, we will focus on the modeling and analysis of the experimentally demonstrated optical devices where DFQW has been used as the active region, so that the modification of both the optical properties and operation wavelength can enhance the device performance. The devices are DFB lasers and waveguide-type optical amplifiers. In Section II, the model of the DFQW structure will be discussed. In Section III, the modification of the operation wavelength of DFQW DFB lasers will be analyzed. In Section IV, the optical properties of polarization-independent optical amplifiers using DFQW will be addressed. Finally, the conclusion will be given in Section V.

## II. MODELING OF DIFFUSED QWs

The calculation of QW band structure has been well established in literature. In this section, we will only present the primary equations that include the effects due to QW intermixing. For QW structures whose compositions include no more than two elements in each group of the Group III and Group V elements, such as  $\text{In}_x\text{Ga}_{1-x}\text{As}_y\text{P}_{1-y}$ , interdiffusion can be described by error functions, according to the Fickian relation. The In and As concentration profiles after interdiffusion  $\tilde{x}(z)$  and  $\tilde{y}(z)$ , respectively, can be written as

$$\tilde{x}(z) = 1 - \frac{1-x}{2} \left[ \text{erf} \left( \frac{L_z + 2z}{4L_d^{\text{III}}} \right) + \text{erf} \left( \frac{L_z - 2z}{4L_d^{\text{III}}} \right) \right] \quad (1)$$

$$\tilde{y}(z) = 1 - \frac{1-y}{2} \left[ \text{erf} \left( \frac{L_z + 2z}{4L_d^{\text{V}}} \right) + \text{erf} \left( \frac{L_z - 2z}{4L_d^{\text{V}}} \right) \right] \quad (2)$$

where  $L_z$  is the well width and  $z$  is the coordinate along the growth direction,  $L_d^{\text{III}}$  and  $L_d^{\text{V}}$  are the diffusion lengths of the Group III and Group V elements, respectively. The ratio of the two diffusion lengths is  $k \equiv L_d^{\text{V}}/L_d^{\text{III}}$ . In the case of InGaAs–InP square QW, the interface of barrier/well will become quaternary material InGaAsP after interdiffusion. These equations are applicable for other QW structures in which only the Group III or Group V elements are involved in interdiffusion such as AlGaAs–GaAs and GaAsP–GaAs QWs. For the former structure, only Al and Ga are involved in interdiffusion and their diffused composition profile are  $\tilde{x}(z)$  and  $1 - \tilde{x}(z)$ , respectively. For the latter case, the diffused composition profile of As and P are  $\tilde{y}(z)$  and  $1 - \tilde{y}(z)$ , respectively. This error function model was compared with experimental results for InGaAsP–InP [4] and AlGaAs–GaAs DFQWs [19], and a good agreement was found.

Apart from the change in composition profile, strains may be generated in the QW structure during the interdiffusion. Considering the interdiffusion of an as-grown lattice-matched  $\text{In}_{0.53}\text{Ga}_{0.47}\text{As}$ –InP QW, tensile strain is generated in the well near the well/barrier interface when compressive strain is created in the barrier near the barrier/well interface. As a result, the bulk potential profiles of the conduction band (C), heavy hole (HH), and light hole (LH), taking into account the effects of composition modification and generated strains, will become

$$V_C(z) = \tilde{V}^C(z) - (1 - Q_c)S_{\perp}(z) \quad (3)$$

$$V_{\text{HH}}(z) = \tilde{V}^V(z) - (1 - Q_c)S_{\perp}(z) + s_{//}(\tilde{x}(z), \tilde{y}(z)) \quad (4)$$

$$\begin{aligned} V_{\text{LH}}(z) = & \tilde{V}^V(z) - (1 - Q_c)S_{\perp}(z) \\ & + 0.5 [s_{//}(\tilde{x}(z), \tilde{y}(z)) + \Delta_0(\tilde{x}(z), \tilde{y}(z))] \\ & - 0.5 \left\{ 9 [s_{//}(\tilde{x}(z), \tilde{y}(z))]^2 + [\Delta_0(\tilde{x}(z), \tilde{y}(z))]^2 \right. \\ & \left. - 2s_{//}(\tilde{x}(z), \tilde{y}(z)) \Delta_0(\tilde{x}(z), \tilde{y}(z)) \right\}^{0.5} \quad (5) \end{aligned}$$

where  $s_{//}(\tilde{x}(z), \tilde{y}(z)) = -b(\tilde{x}(z), \tilde{y}(z))[1 + 2c_{12}(\tilde{x}(z), \tilde{y}(z))/c_{11}(\tilde{x}(z), \tilde{y}(z))]\varepsilon(\tilde{x}(z), \tilde{y}(z))$ .  $\tilde{V}^C(z)$  and  $\tilde{V}^V(z)$  are the diffused potential profiles of the conduction band and valence band, respectively.  $Q_c$  is the conduction band offset ratio.  $S_{\perp}$  is the biaxial component of the strain. The third term of (4) and the last two terms of (5) are the splitting energy of the HH and LH induced by the uniaxial component of the strain, respectively [14], [20].  $b(\tilde{x}(z), \tilde{y}(z))$  and  $\varepsilon(\tilde{x}(z), \tilde{y}(z))$  are the shear deformation potential and the biaxial hydrostatic stress, respectively.  $\Delta_0(\tilde{x}(z), \tilde{y}(z))$  is the spin-orbit splitting.  $c_{ij}$  are the elastic constants. Following the  $k \cdot p$  method, (4) and (5) have been substituted to the  $4 \times 4$  Luttinger–Kohn Hamiltonian [11] for determining the subband structures of HH and LH so that the coupling between HH and LH, i.e., bandmixing effect, can be taken into account. Meanwhile, (3) is applied to one-particle Schrödinger-like equation for calculating the conduction band. Since injected carriers will modify the band structure, Poisson's equation has to be solved self-consistently with the subband model [14].

With the subband structure, the optical properties of DFQW can be modeled [11], [22]. Using the density matrix theory, the material gain  $g(\hbar\omega)$  and the change in refractive index  $\Delta n(\hbar\omega)$  can be obtained as

$$\begin{aligned} g(\hbar\omega) = & \frac{2m_r\omega}{n_{\text{eff}}c\varepsilon_0\pi\hbar^2L_z} \sum_{n,m} \int_0^{\infty} dE_{//} |e \cdot M_{cv}(E_{//})|^2 \\ & \times \frac{\frac{\hbar}{\pi\tau_{in}}}{(E_{en} - E_{hm} + E_{//} - \hbar\omega)^2 + \left(\frac{\hbar}{\tau_{in}}\right)^2} \\ & \times [f_c^n(E_{//}) - f_v^m(E_{//})] \quad (6) \end{aligned}$$

$$\begin{aligned} \Delta n(\hbar\omega) = & \frac{m_r}{n_{\text{eff}}c\varepsilon_0\pi\hbar^2L_z} \sum_{n,m} \int_0^{\infty} dE_{//} |e \cdot M_{cv}(E_{//})|^2 \\ & \times \frac{E_{en} - E_{hm} + E_{//} - \hbar\omega}{(E_{en} - E_{hm} + E_{//} - \hbar\omega)^2 + \left(\frac{\hbar}{\tau_{in}}\right)^2} \\ & \times [f_c^n(E_{//}) - f_v^m(E_{//})] \quad (7) \end{aligned}$$

where  $|e \cdot M_{cv}(E_{//})|^2$  is the optical matrix element and  $f_c^n(E_{//})$ ,  $f_v^m(E_{//})$  are the Fermi distribution functions for electrons and holes, respectively.  $E_{//}$  is the total kinetic energy of an electron-hole pair due to motion perpendicular to the crystal growth direction.  $E_{en}$  and  $E_{hm}$  are, respectively, the  $n$ th electron subband and the  $m$ th hole subband energies.  $\hbar\omega$  is the photon energy,  $m_r$  is the electron-hole reduced mass, and  $\tau_{in}$  is the relaxation time. The total complex refractive index in the well layer is given by

$$n(\hbar\omega) = n_2(\hbar\omega) + \Delta n(\hbar\omega) + i \frac{g(\hbar\omega)}{2k_0}. \quad (8)$$

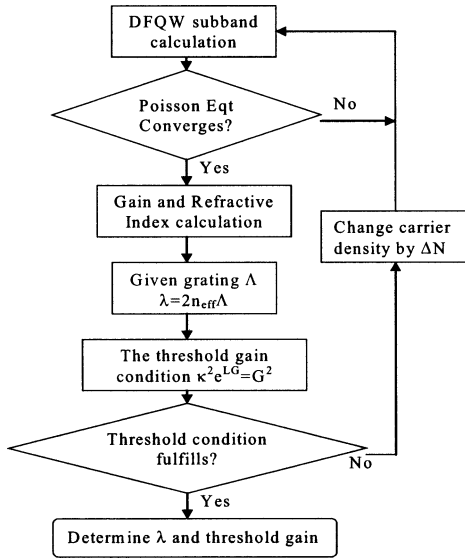


Fig. 1. Flowchart of the self-consistent model for determination of operation wavelength and threshold gain of diffused QW DFB laser.  $\kappa = 20 \text{ cm}^{-1}$  is used in simulation. DFB laser length  $L = 400 \mu\text{m}$ ,  $\Delta N$  is the change in carrier density, and  $n_{\text{eff}}$  is the effective refractive index of the laser structure.

### III. DIFFUSED QW DFB LASER

A DFB laser using DFQW as the active region has recently been studied experimentally to demonstrate the tuning of emission wavelength by intermixing the QW active region to become a DFQW [21]. The adjustment of emission wavelength due to QW intermixing has also been modeled [22], [23]. Fig. 1 shows a flowchart that illustrates the model used in [22] and [23] to determine the emission wavelength. To determine the emission wavelength of the DFQW DFB laser, equations for QW band structure, emission wavelength, and lasing threshold have to be solved self-consistently. The upper part of the flowchart shows the self-consistent loop in which the DFQW subband structure is determined by solving self-consistently the  $k \cdot p$  model equations with the Poisson equation [14] as discussed in Section II.

The lower part of the flowchart shows the self-consistent loop used to determine the emission wavelength. The emission wavelength must satisfy the following two equations simultaneously and, therefore, should be determined using a self-consistent loop. The first equation gives the relation between the emission wavelength and the period of the diffraction grating as

$$\lambda = 2n_{\text{eff}}\Lambda \quad (9)$$

where  $\Lambda$  is the grating period and  $n_{\text{eff}}$  is the effective refractive index of the guided mode in the laser structure. The optical guided mode and  $n_{\text{eff}}$  are determined using the transfer matrix technique based on the equivalent attenuated vector theory [22]. In a  $\lambda/4$  DFB laser, the oscillation frequency locates at the Bragg frequency exactly and the detuning parameter is zero. Since  $n_{\text{eff}}$  is a function of photon energy (or wavelength), the emission wavelength that satisfies (9) can be graphically determined by the intersection of the  $n_{\text{eff}}$  spectrum and the equation  $n_{\text{eff}} = hc/2\Lambda E$  as in Fig. 2. When the QW is intermixed, the bandgap and the effective refractive index spectrum are

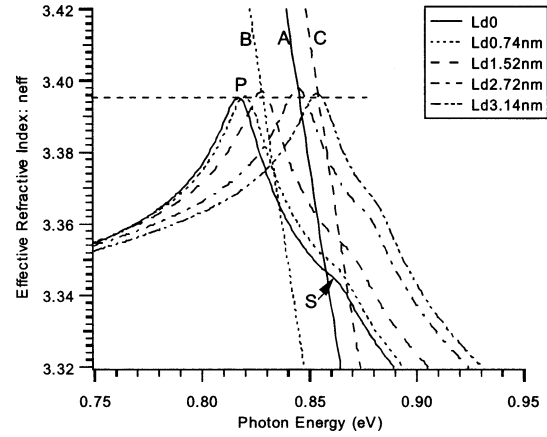


Fig. 2. Effective refractive index spectrum of DFB lasers using DFQW as the active region. Lines A, B, and C are for the grating period of 0.218, 0.224, and 0.214  $\mu\text{m}$ , respectively. The carrier densities for  $L_d = 0, 0.74, 1.52, 2.72,$  and  $3.14 \text{ nm}$  are  $4.2 \times 10^{12} \text{ cm}^{-2}$ ,  $4.3 \times 10^{12} \text{ cm}^{-2}$ ,  $4.5 \times 10^{12} \text{ cm}^{-2}$ ,  $4.9 \times 10^{12} \text{ cm}^{-2}$ , and  $5.3 \times 10^{12} \text{ cm}^{-2}$ , respectively.

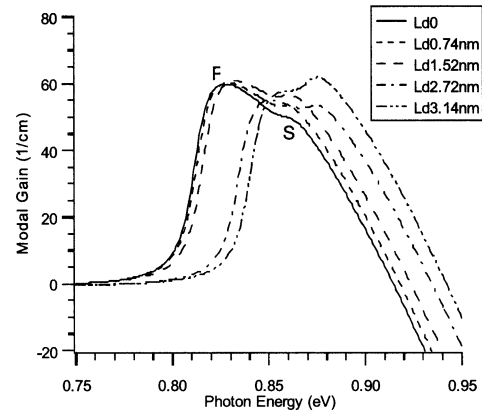


Fig. 3. Modal gain spectrum of the DFB laser using DFQW as the active region. The carrier densities for  $L_d = 0, 0.74, 1.52, 2.72,$  and  $3.14 \text{ nm}$  are  $4.2 \times 10^{12} \text{ cm}^{-2}$ ,  $4.3 \times 10^{12} \text{ cm}^{-2}$ ,  $4.5 \times 10^{12} \text{ cm}^{-2}$ ,  $4.9 \times 10^{12} \text{ cm}^{-2}$ , and  $5.3 \times 10^{12} \text{ cm}^{-2}$ , respectively.

blue-shifted (i.e., the photon energy increases). As a result, the intersection points and the emission wavelength in Fig. 2 shift. This is the main mechanism responsible for the tuning of emission wavelength by QW intermixing.

The second equation gives the lasing threshold of the modal gain at the emission wavelength in terms of structural parameters

$$\kappa^2 e^{GL} = G^2 \quad (10)$$

where  $\kappa$  is the coupling coefficient per unit length,  $L$  is the total length of the DFB laser, and  $G$  is the threshold modal gain. Equation (10) is obtained in the weak-coupling regime by solving the coupled-wave theory [24], assuming that the DFB laser is connected to a waveguide and there are no sharp boundaries at the two ends of the grating. Since the modal gain is a function of photon energy, the emission wavelength with a modal gain that satisfies (10) can be obtained by drawing a horizontal line that represents the threshold modal gain and finding its intersection with the modal gain spectrum in Fig. 3. The threshold modal gain can be determined from (10) by putting in the suitable structural parameters  $\kappa$  and  $L$ .

The determination of the emission wavelength requires going around the self-consistent loops of the subband structure and threshold condition as shown in Fig. 1 until the threshold conditions described by both (9) and (10) are satisfied by the same emission wavelength. A detailed discussion of this self-consistent calculation can be found in [14], [22], and [23]. In general, the self-consistent simulation is very inconvenient and time consuming. Tremendous saving in modeling and computational effort can be achieved if there is a simple model or design rule to determine the tuning range of the emission wavelength without the self-consistent calculation steps.

In the present section, we have four objectives.

- 1) To propose a *simple design rule* that can be used to estimate the relationship between the grating period and tuning range due to QW intermixing without any complicated numerical simulation as discussed above. The design rule is particularly useful for lasers operated around the threshold condition, at which the peak gain approximately equals the loss of the structure.
- 2) To show the *validity of the simple design rule*. The sensitivity of the design rule to any variations of carrier density will be addressed and a comparison of the results from the design rule and the self-consistent model will be made.
- 3) We also discuss *the range of grating period in which the design rule can be applied*.
- 4) In addition, *the effects of any deviations in the grating period on the tunable wavelength range by using DFQW* will be discussed.

To help the discussion of the simple design rule, we discuss briefly the mechanism responsible for limiting the tuning range of the emission wavelengths. A detailed discussion of the mechanism can be found in [22] and [23]. Figs. 2 and 3 show the DFQW effective refractive index and modal gain spectra, respectively, calculated using the self-consistent loop in the upper part of the flowchart in Fig. 1. The active layer of the laser consists of five  $\text{In}_{1-x}\text{Ga}_x\text{As}_y\text{P}_{1-y}$  quantum wells ( $x = 0.269$  and  $y = 0.79$  for well;  $x = 0.235$  and  $y = 0.512$  for barrier; the well and barrier widths equal 10 nm). As shown in Fig. 2, lines A, B, and C plot the equation  $n_{\text{eff}} = hc/2\Delta E$  for three different values of grating period shown in the caption. For the grating period represented by line A ( $\Lambda = 0.218 \mu\text{m}$ ), the emission wavelength of the DFB laser with an as-grown QW structure is 0.8574 eV. When the QW is intermixed with  $L_d = L_d^{\text{III}} = L_d^{\text{V}}$ , the refractive index and gain spectra are blue-shifted (i.e., the photon energy increases) because of the increase of bandgap energy through QW intermixing. However, since the emission wavelength is determined by the intersection of DFQW refractive index spectra and (9), the emission wavelength is red-shifted while the refractive index spectrum is blue-shifted. The maximum tuning range achievable for this grating period is 21.2 nm when  $L_d$  changes from 0 (i.e., as-grown QW) to 2.72 nm because the grating line A intersects the refractive index spectrum of  $L_d = 2.72$  nm at its peak. When the QW is further interdiffused to  $L_d = 3.14$  nm, the refractive index spectrum is over-shifted so that the tuning range reduces to 18.6 nm and the emission wavelength shifts backward (blue-shifted) from 0.845 to 0.847 eV. A summary

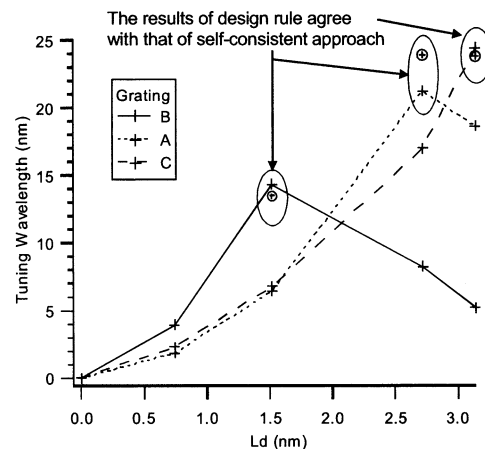


Fig. 4. Tuning range of the DFQW DFB lasers. A, B, and C denote the grating period of 0.218, 0.224, and 0.214  $\mu\text{m}$ , respectively. The symbol  $\oplus$  denotes the maximum tuning range estimated using the design rule.

of the wavelength tuning range for different  $L_d$ s are shown in Fig. 4. Here, we do not discuss in detail the self-consistent calculation, although it is used to obtain these results, owing to limitation in space.

#### A. Simple Design Rule

The design rule proposed here is a simple method or approach that can be used to estimate the wavelength tuning range for a given grating period without involving the laborious self-consistent calculation described previously. Through the design rule, the maximum tuning range can be determined simply based on the effective refractive index spectrum of  $L_d = 0$ . It is possible to develop a simple design rule because there are some universal features in the effective refractive index spectrum and modal gain spectrum. Three universal features are identified from the theoretical results shown in [22] and [23]. The first universal feature is observed in the effective refractive index spectrum for the QW structure with  $L_d = 0.74$  nm shown in [22, Fig. 1]. In the figure, when the carrier density is increased, the refractive index spectrum is generally shifted upward without significant broadening of the spectrum. The second universal feature is that the line representing the equation  $n_{\text{eff}} = hc/2\Delta E$  (hereafter, we call this line the grating line) in Fig. 2 is straight and very steep. The third universal feature is that when  $L_d$  increases and gain spectrum blue shifts as shown in Fig. 3, the refractive index also blue-shifts more or less horizontally without significant change in the peak index value as shown in Fig. 2. In the following paragraphs, these universal features are used to set up a simple design rule so that the tuning range can be estimated without any self-consistent calculation.

We first use the third universal feature to establish the simple design rule. The first and second features will be used to establish the range of validity of this design rule. According to the third universal feature, when the QW is intermixed, the effective refractive index spectrum is shifted horizontally without significant broadening or modifications to the shape of the spectrum. As shown in Fig. 2, once the grating period is fixed, the tuning range mainly depends on the shift of the refractive index spectrum due to QW interdiffusion. For the grating period of

0.218  $\mu\text{m}$  represented by line A, the maximum tuning range is reached when the refractive index spectrum shifts to such a stage that its peak intersects with line A (this happens when  $L_d$  equals 2.72 nm). The tuning range cannot be increased even if we use a larger value of  $L_d$  owing to the decrease in refractive index beyond the peak of the spectrum. From this observation, the maximum tuning range can be estimated by horizontally shifting the refractive index spectrum for  $L_d = 0$  (by applying the third universal feature) until the peak of the spectrum intersecting line A. Using this technique, we can find the maximum tuning range approximately without calculating the refractive index spectrum for other  $L_d$ s.

A further simplification of the design rule is possible based on the third universal feature again. When the bandgap is blue-shifted by QW intermixing, the refractive index spectrum is blue-shifted without significant changes in the shape and peak of the spectrum. Therefore, we can estimate the maximum tuning range by drawing a horizontal line that is tangential to the peak of the refractive index spectrum for  $L_d = 0$  nm, as shown in Fig. 2. The intersection point of this horizontal tangential line and line A gives the lower bound of the emission photon energy obtained using this grating period. Using this technique, we do not need to shift the refractive index spectrum horizontally to find the maximum tuning range. The simple design rule can thus be summarized as follows. *The maximum tuning range can be found from the following two intersection points: intersection of the grating line and the effective refractive index spectrum for  $L_d = 0$ , and intersection of the grating line and the horizontal line tangential to the peak of the effective refractive index spectrum.* With this design rule, one can quickly estimate the maximum wavelength tuning range based on the refractive index spectrum for  $L_d = 0$  and the grating line.

### B. Validity of the Design Rule

One important question about this design rule is whether the accuracy of the estimation is affected by a small change in carrier density. This is an important question because any changes in laser structures can modify the threshold carrier concentration. In general, it is time consuming to find the exact carrier density that satisfies the threshold condition. If the tuning range estimated using the design rule is not strongly affected by a change in carrier density, we can find the carrier density that approximately satisfies the threshold condition without any complicated and time-consuming computation.

Here, we use the first and second universal features to show that the estimated maximum tuning range is not affected significantly by small changes in carrier density. Consider the schematic diagram for the effective refractive index spectrum shown in Fig. 5. In the figure, two effective refractive index spectra are shown for two different carrier densities. The emission wavelength is given by the intersection point of the spectra for  $L_d = 0$  with the grating line. Here,  $\lambda_1$  and  $\lambda_2$  denote the wavelengths of the intersection of the grating line and the refractive index spectra for the low and high carrier densities.  $\lambda_3$  and  $\lambda_4$  denote the wavelengths of the intersection points of the horizontal tangential lines at the peaks of the two spectra and the grating line. Since the grating line is straight and steep (second universal feature) and the refractive index

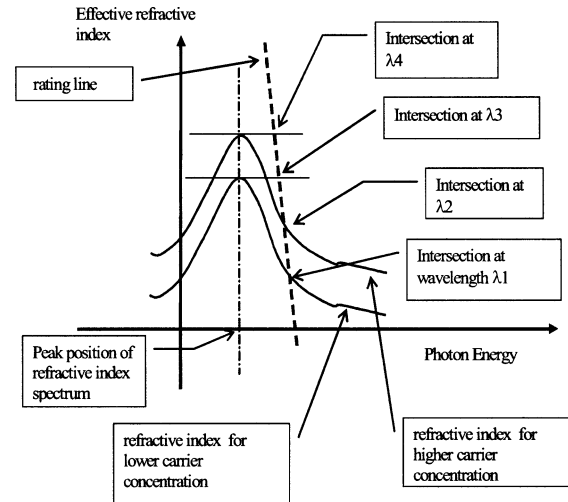


Fig. 5. Schematic diagram of the refractive index spectra at two different carrier densities.

spectrum moves upward without significant broadening when the carrier density increases (first universal feature 1),  $\lambda_1 - \lambda_3$  approximately equals  $\lambda_2 - \lambda_4$ . In other words, the estimated maximum tuning range is not sensitive to any small change in carrier density. We, therefore, can use the carrier density that approximately satisfies the threshold condition to estimate the maximum wavelength tuning range for a particular grating period.

To find the approximate carrier density, we can adjust the carrier density so that the gain in the plateau region in the modal gain spectrum approximately equals the threshold gain determined from (10). For example, the modal gain spectra shown in Fig. 3 have their peak gain values approximately equal  $51.7 \text{ cm}^{-1}$ , which is the threshold modal gain for  $\kappa = 20 \text{ cm}^{-1}$  and  $L = 400 \mu\text{m}$ . In this case, the estimated carrier density of  $L_d = 0, 0.74, 1.52, 2.72,$  and  $3.14 \text{ nm}$  are  $4.2 \times 10^{12} \text{ cm}^{-2}$ ,  $4.3 \times 10^{12} \text{ cm}^{-2}$ ,  $4.5 \times 10^{12} \text{ cm}^{-2}$ ,  $4.9 \times 10^{12} \text{ cm}^{-2}$ , and  $5.3 \times 10^{12} \text{ cm}^{-2}$ , respectively.

To show the validity of the design rule, the results obtained from the design rule are compared with those from self-consistent calculation. As shown in Fig. 2, the refractive index spectra are obtained with carrier densities that approximately satisfy the threshold condition (a modal gain of  $51.7 \text{ cm}^{-1}$ ). A horizontal tangential line is drawn at the peak of the spectrum for  $L_d = 0$ . This horizontal line cuts the grating line A, B, C for different values of grating period. When  $\Lambda$  equals 0.218  $\mu\text{m}$  (Line A), the maximum tuning range equals 24.3 nm. Similarly, when  $\Lambda$  equals 0.224  $\mu\text{m}$  (Line B) and 0.214  $\mu\text{m}$  (Line C), the maximum tuning range equals 14.3 and 24.4 nm, respectively. These estimated tuning ranges are plotted in Fig. 4 and compared with the maximum tuning range of the corresponding grating period determined through a self-consistent approach. In general, there is a good agreement between the self-consistent calculation and the simple design rule.

### C. Range of Grating Period Used in the Design

Although in the paragraphs above we discuss the simple design rule that can be used to find the maximum tuning range, there is still a need of a guideline that helps us to estimate the

range of grating period where the simple design rule can be applied without carrying out any self-consistent calculation. To establish this guideline, we need to analyze Figs. 2 and 3 in detail. In the effective refractive index spectrum of  $L_d = 0$  shown in Fig. 2, there are a peak (labeled P) and a shoulder (labeled S). As one can observe in Fig. 3, the gain region between P and S is relatively flat (a plateau in the spectrum) and close to the top of the gain spectra. Therefore, the injected carrier density can be minimized by choosing a value of grating period  $\Lambda$ , so that the emission wavelength lies within this region. The simple design rule can be applied to these grating periods, which have emission wavelengths lying within this plateau region (i.e., the intersection of the grating line and the refractive index spectrum lies between points P and S). Within this region, the gain spectrum is relatively flat and we only need to change the carrier density by a small amount to satisfy the threshold condition when we modify the grating period. As a result, the simple design rule can be applied to grating periods with intersection points lying between points S and P.

#### D. Effects of Any Grating Deviation

In the fabrication process, the actual grating period  $\Lambda$  produced may deviate from the expected value and, thus, causes a deviation in the maximum tuning range of the DFQW DFB laser. Therefore, it is useful to estimate the error in the maximum tuning range caused by any deviations in the grating period. For the case of  $\Lambda = 0.218 \mu\text{m}$  (Line A), assuming that there is  $\pm 6 \times 10^{-4} \mu\text{m}$  deviation in the grating period, i.e.,  $\Lambda$  becomes  $0.2174$  or  $0.2186 \mu\text{m}$ . The emitted photon energy will change by  $+3$  and  $-3$  meV, respectively. From the intersects of the grating lines ( $\Lambda = 0.2174$  and  $0.2186 \mu\text{m}$ ) and the refractive index spectra, it is found that the resulting errors in the maximum tuning range are  $+0.5$  and  $-0.5$  nm, respectively. Since at the emission wavelength for the as-grown structure ( $L_d = 0$ ) the refractive index decreases when the photon energy increases, any increase in the emitted photon energy for the as-grown structure due to a decrease in the grating period results in an increase in the tuning range. Similarly, any increase in the grating period results in a red-shift of the emitted photon energy of the as-grown structure and a decrease in the maximum tuning range. In addition, the error of the tuning range due to errors in the grating period depends on the slope of the refractive index spectra. The steeper is the refractive index spectrum, the larger is the variation of the tuning range. As a consequence, errors in the grating period cause deviations in the tuning range, which is linearly proportional to the slope of the refractive spectra.

#### IV. POLARIZATION-INDEPENDENT OPTICAL AMPLIFIERS USING DIFFUSED QW

Different types of QW structures have been used as the active region of optical devices because of their enhanced optical properties, compared with conventional semiconductor heterostructure materials. However, there is a well-known inherent feature of QW structures for these applications, which is TE and TM polarization dependence, due to the nondegeneracy of HH and LH in the growth direction. To tackle this problem, one of the methods is to make use of a “parabolic-like” QW structure so

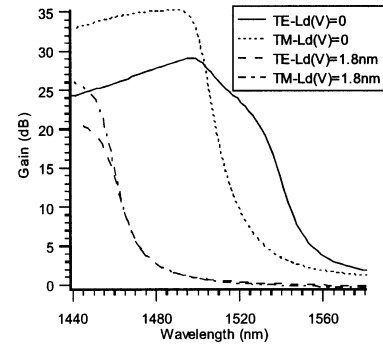


Fig. 6. TE and TM gain spectra of  $\text{In}_{0.53}\text{Ga}_{0.47}\text{As}-\text{In}_{0.74}\text{Ga}_{0.26}\text{As}_{0.57}\text{P}_{0.43}$  QW with carrier density of  $9 \times 10^{12} \text{ cm}^{-2}$ . The well width is 6 nm. The  $L_d^V$  of the diffused QW is 1.8 nm and the diffusion ratio is  $k = 2$ .

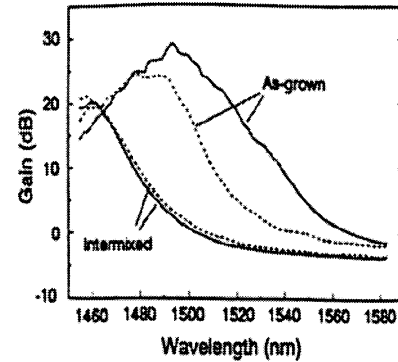


Fig. 7. Experimental polarization-independent gain spectra from [4] with the same QW structure. Solid line denotes TE gain and dotted line denotes TM gain.

that the quantum confinement Stark shift becomes insensitive to the masses of the carriers [25], [26]. This method is useful for QW modulators but not for QW optical amplifiers. Another idea is to introduce appropriate strains in wells and barriers so that HH1 and LH1 eigenstates merge together to achieve polarization independence [27]. Recently, QW intermixing has been theoretically proposed [28] and experimentally demonstrated [4] to generate suitable tensile strain in the well so that HH1 and LH1 merge to eliminate the polarization dependence, taking advantage of the simple post-growth modification technique of QW intermixing. In this section, new simulation results are presented for the DFQW structure that has been experimentally demonstrated for providing polarization-independent optical gain, with a detailed analysis and discussion.

The theoretical TE and TM gain spectra before and after QW intermixing are shown in Fig. 6, which are in very good agreement with the experimental results shown in Fig. 7. The as-grown QW structure is lattice-matched  $\text{In}_{0.53}\text{Ga}_{0.47}\text{As}(\text{well})/\text{In}_{0.74}\text{Ga}_{0.26}\text{As}_{0.57}\text{P}_{0.43}(\text{barrier})$  structure and the well width considered is 6 nm. The optical confinement is considered as  $\sim 0.01$ . After QW intermixing with  $L_d^V = 1.8$  nm and  $k = 2$ , the TE and TM gain spectra merge together to provide polarization-independent optical amplification. This value of  $k$  is obtained by adjusting its value until the theoretical gain spectra agree with the experimental spectra. The value of  $k$  obtained here agrees with the value obtained in [4]. When  $L_d^V = 0$ , the eigenstates of LH and HH are nondegenerate at  $k_{//} = 0$  with an energy difference of

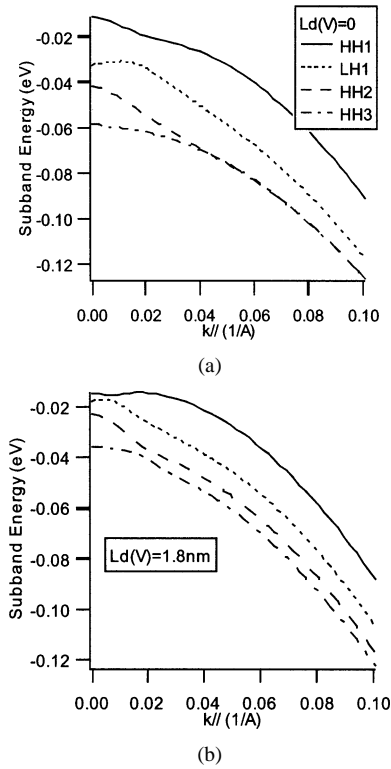


Fig. 8. Subband structure of the valence band of the diffused QW structure with: (a)  $L_d^V = 0$  and (b)  $L_d^V = 1.8$  nm.

21 meV, as shown in Fig. 8(a). The TE and TM gain spectra clearly separate from each other because the optical matrix element (OME) of TE gain is nonzero for both the LH and HH subbands, while the OME of TM gain is nonzero only for the LH subbands and zero for HH subbands [14]. In Fig. 6, the peak and shoulder in the TE gain spectrum at  $\sim 1500$  and  $1540 \mu\text{m}$  are due to the C1-HH1 and C1-LH1 transitions, respectively. They can also be observed in experiment, as shown in Fig. 7. When  $L_d^V$  increases to 1.8 nm, HH1 and LH1 subbands move close to each other with less than 3 meV energy difference [see Fig. 8(b)], leading to polarization-independent optical gain.

The TE and TM gain of the polarization-independent DFQW merge together at the long-wavelength tail ( $> 1460 \mu\text{m}$ ). However, they split in the short-wavelength region ( $< 1460 \mu\text{m}$ ), which is an important feature in a polarization-independent device. In order to understand this feature, we study in detail the OME, Fermi occupation factor, and joint density of state (JDOS), which are the three main factors of the material gain given by (6). In Fig. 9, we plot the OME as a function of  $k_{//}$  for the following two cases: (a)  $L_d^V = 0$ , and (b)  $L_d^V = 1.8$  nm,  $k = 2$ . The features of OME are quite similar in these two cases. When  $k_{//} \rightarrow 0$ , OME of the TE mode mainly comes from the C1-HH1 and C1-LH1 transitions. The OME of TM mode mainly comes from the C1-LH1 transitions, and the OME of C1-HH1 transition for the TM mode is very close to zero. When  $k_{//}$  increases, owing to band mixing and a smaller HH effective mass in the  $x$ - $y$  plane, the lowest valence subband, HH1, has more and more LH characteristics. On the other hand, LH1 has more and more HH characteristics when  $k_{//}$  increases. As a result, OME of C1-HH1 transition for TE mode decreases, but increases for TM mode as shown

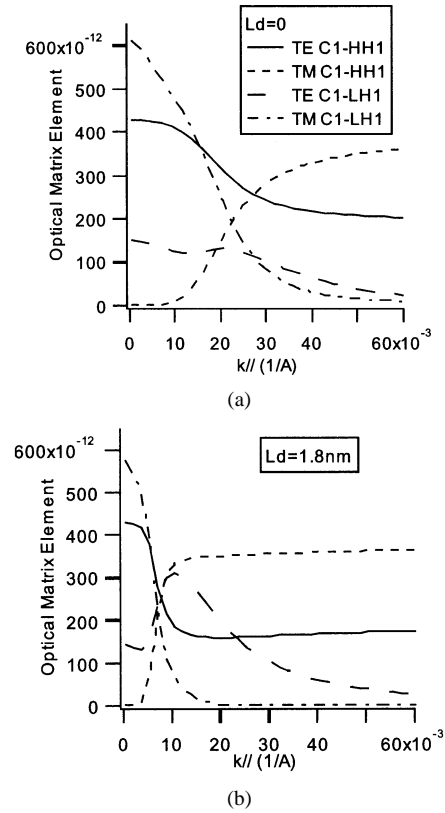


Fig. 9. Optical matrix element of the diffused QW structure. (a)  $L_d^V = 0$ . (b)  $L_d^V = 1.8$  nm.

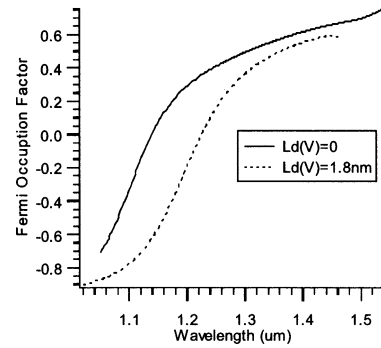


Fig. 10. Fermi occupation factor of the diffused QW structure.

in Fig. 9. Similarly, the OME of C1-LH1 transition for TE mode increases, but decreases for TM mode. We notice that around  $k_{//} = 0$ , the OME for the TE mode equals the OME of TM mode (obtained by adding the OME of C1-HH1 and C1-LH1 transitions for each mode). It is, therefore, not possible to use the features found in the TE and TM OME to explain the difference in TM and TE gain in the short-wavelength region in the polarization-independent optical amplifier. Other factors have to be considered. In Fig. 10, we show the Fermi occupation factor. In general, the Fermi occupation factor of  $L_d^V = 0$  is higher than that of  $L_d^V = 1.8$  nm. This explains why the TE and TM gain spectra for the case of  $L_d^V = 0$  is higher than the  $L_d^V = 1.8$  nm gain spectra. However, the Fermi occupation factor also cannot explain why in the short wavelength region the TM gain is higher than the TE gain, as it affects both the TE and TM gain equally.

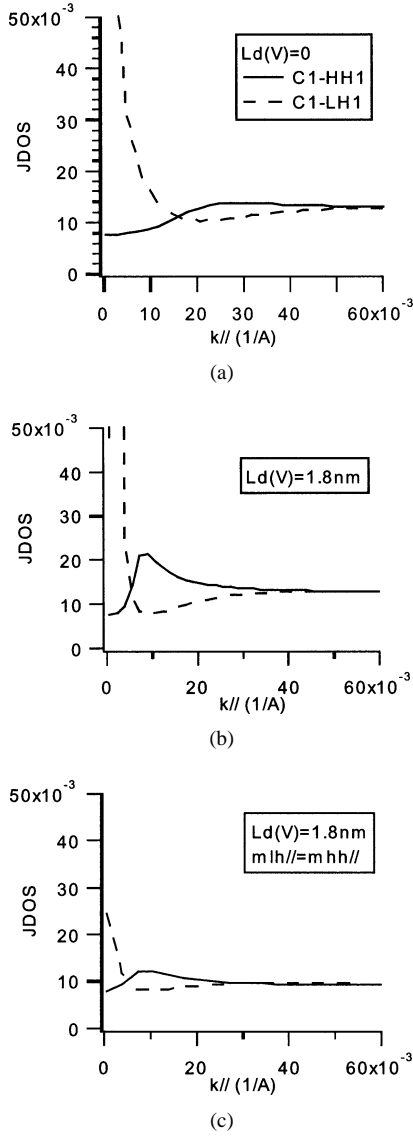


Fig. 11. JDOS of the diffused QW structure. (a)  $L_d^V = 0$ , (b)  $L_d^V = 1.8$  nm, and (c)  $L_d^V = 1.8$  nm with  $m_{hh//} = m_{lh//}$ .

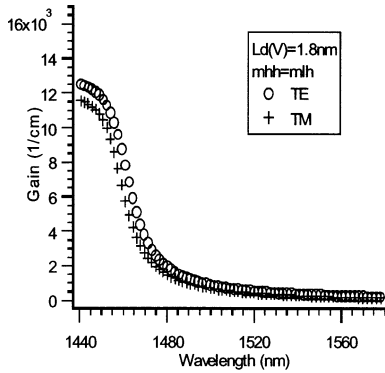


Fig. 12. TE and TM gain spectra of the diffused QW with  $L_d^V = 1.8$  nm,  $k = 2$  and  $m_{hh//} = m_{lh//}$ .

We show the last factor of material gain: JDOS in Fig. 11. Its effects on the gain spectrum can be understood by studying the C1-HH1 JDOS as shown in Fig. 11(a) and (b). For both the cases of  $L_d^V = 0$  and  $L_d^V = 1.8$  nm, when  $k_{//} \rightarrow 0$ , the first subband is HH like and the HH effective mass in the  $x$ - $y$  plane

( $m_{hh//}$ ) is small; therefore, the JDOS of C1-HH1 is small with a value of  $\sim 0.0075$ . On the other hand, the JDOS of C1-LH1 is very large in this region. However, when  $k_{//}$  increases, HH1 becomes more LH-like. This change from HH to LH characteristics can be confirmed from the increase in the TM OME of C1-HH1 shown by dashed lines in Fig. 9(a) and (b) (this occurs when  $k_{//} > 0.02$  for  $L_d^V = 0$  and  $k_{//} > 0.01$  for  $L_d^V = 1.8$  nm). We expect to find an increase in JDOS for this change from HH to LH characteristics, because the LH effective mass in the  $x$ - $y$  plane ( $m_{lh//}$ ) and the JDOS is larger than those of HH. In Fig. 11, the JDOS of C1-HH1 is almost double,  $\sim 0.013$ – $0.014$ , when  $k_{//} > 0.02$  for  $L_d^V = 0$  (as compared to the value at  $k_{//} = 0$ ) and  $k_{//} > 0.01$  for  $L_d^V = 1.8$  nm. Since the gain is proportional to the JDOS and there is a higher JDOS for the C1-LH1 transition near to the edge of the subband ( $k_{//} = 0$ ), the TM gain near to the subband edge is larger than the TE gain in the case of  $L_d^V = 1.8$  nm. For very large  $k_{//}$  ( $> 0.02$ ), the JDOS for C1-HH1 and C1-LH1 transitions are nearly identical. However, in this range of  $k_{//}$ , the OME of TM mode is about twice the OME of TE mode according to Fig. 9(b). As a consequence the TM gain is still larger than the TE gain in this regime.

To confirm our explanation that JDOS is the main factor responsible for the difference in TE and TM gain, we calculate and plot the JDOS by assuming  $m_{hh//} = m_{lh//}$  in Fig. 11(c). The JDOS of C1-HH1 and C1-LH1 transitions obtained in this way are closer in value for a wide range of value of  $k_{//}$  than those shown in Fig. 11(a) and (b). We also calculated the TE and TM gain spectra by assuming  $m_{hh//} = m_{lh//}$  and plotted them in Fig. 12. The TE and TM gain spectra are close in value in a wide range of wavelength, and the difference in TE and TM gain above  $1460$   $\mu\text{m}$  is very small. This shows that by putting the HH's and LH's effective mass in the  $x$ - $y$  plane, the difference in TE and TM gain can be eliminated.

To conclude, we successfully explain why the TE and TM gain of polarization-independent DFQW can only merge at the long-wavelength tail of the gain spectrum when enough tensile strain is generated by QW intermixing to make HH1 and LH1 degenerate in energy. The main reason for this phenomenon is that, in QWs,  $m_{hh//} \neq m_{lh//}$  in the  $x$ - $y$  plane. This problem is difficult to remove, as it is an intrinsic property of QW structures. This explanation not only applies to tensile-strained DFQWs, but also to other tensile-strained QWs designed for polarization-independent application.

It should be noted that, in the experimental result, TM gain also shows higher values even though it is not as clear as in the theoretical results. This may be due to the higher loss of TM polarized light (normal to the plane of QW) from the defects of the top surface and metallization of the device structure. In the theoretical results, there is a singularity in the JDOS of C1-LH1 when  $k_{//} \rightarrow 0$  because there is a strong repulsion between LH1 and HH2 in this region and the slope of LH1 subband is close to zero. However, since the singularity happens in a very narrow range of  $k_{//}$  and its effect is usually reduced by broadening, the singularity does not appear in the TM gain spectrum.

It is interesting to note that apart from the polarization-independent optical amplifier, the polarization-independent



electroabsorption modulator has been demonstrated both experimentally [29] and theoretically [30] using the same principle, i.e., utilizing the tensile strain in wells induced by QW intermixing.

## V. CONCLUSION

In this paper, we have analyzed the optical devices using DFQW as the active region, which have been recently experimentally and theoretically investigated. For the DFQW DFB laser, we proposed a simple design rule to simplify the estimation of maximum tuning range of emission wavelength. We also discuss the validity of the design rule and provide the range of grating period that can be used in a DFQW DFB structure. The proposed design rule and the analysis are very useful for engineering design without involving the complicated self-consistent simulation. We have also discussed the features of polarization-independent optical properties achieved by QW intermixing. Our theoretical results successfully show that polarization independence is achieved by merging HH1 and LH1 through QW intermixing induced tensile strain in the wells. A larger TM gain and absorption is found in photon energies just above the subband edge owing to a larger effective mass of LH in the  $x$ - $y$  plane. This explanation can also be applied to other tensile strained QWs designed for polarization independence. The analysis is valuable for optimizing the performance of polarization-independent DFQW optical devices. Although DFQW optical devices are still in an early stage of development, particularly for those devices using DFQW as the active region, the results obtained so far demonstrate that QW intermixing is a practical and simple technology to enhance the device performance by operation wavelength tuning and reducing polarization dependence.

## REFERENCES

- [1] W. D. Laidig, N. Holoyak, Jr., M. D. Camras, K. Hess, J. J. Coleman, P. D. Dapkus, and J. Bardeen, "Disorder of an AlAs-GaAs superlattice by impurity diffusion," *Appl. Phys. Lett.*, vol. 38, pp. 776-778, 1981.
- [2] E. H. Li, Ed., *Semiconductor Quantum Wells Intermixing*. New York: Gordon and Breach, 2000.
- [3] K. Kawasaki, M. Kubota, Y. Kuze, S. Yamamura, K. Shigihara, Y. Nagai, M. Miyashita, A. Takemoto, and H. Higuchi, "High power ridge waveguide 1.02 mm laser diodes with window structure," in *Proc. ECOC*, Madrid, Spain, 1998, p. 241.
- [4] J. J. He, S. Charbonneau, P. J. Poole, G. C. Aers, Y. Feng, E. S. Koteles, R. D. Goldberg, and I. V. Mitchell, "Polarization insensitive InGaAs/InGaAsP/InP amplifiers using quantum well intermixing," *Appl. Phys. Lett.*, vol. 69, pp. 562-564, 1996.
- [5] W. C. H. Choy, J. J. He, M. Li, Y. Feng, and E. S. Koteles, "InGaAs/InGaAsP diffused QW optical amplifiers and modulators," *Proc. SPIE*, vol. 4277, pp. 69-76, 2001.
- [6] D. H. Yeo, K. H. Yoon, H. R. Kim, and S. J. Kim, "Integration of waveguide type wavelength demultiplexing photodetectors by selective intermixing of InGaAs/InGaAsP quantum well structure," *Proc. SPIE*, vol. 4078, pp. 313-319, 2000.
- [7] J. J. Dubowski, Y. Feng, P. J. Poole, M. Buchanan, S. Poirier, J. Genest, and V. Aimez, "Monolithic multiple wavelength ridge waveguide laser array fabricated by Nd:YAG laser induced quantum well intermixing," *J. Vac. Sci. Technol. A*, vol. 20, pp. 1426-1429, 2002.
- [8] M. J. Lederer, V. Kolev, B. Luther-Davies, H. H. Tan, and C. Jagadish, "Ion-implanted InGaAs single quantum well semiconductor saturable absorber mirrors for passive mode-locking," *J. Phys. D, Appl. Phys.*, vol. 34, pp. 2455-2464, 2001.
- [9] O. M. Khreis, K. P. Homewood, and W. P. Gillin, "Interdiffusion in InGaAs/GaAs: the effect of growth conditions," *J. Appl. Phys.*, vol. 84, pp. 232-236, 1998.
- [10] B. C. Qui, X. F. Liu, M. L. Ke, H. K. Lee, A. C. Bryce, J. S. Aitchison, J. H. Marsh, and C. B. Button, "Monolithic fabrication of  $2 \times 2$  crosspoint switches in InGaAs-InAlGaAs multiple quantum wells using quantum-well intermixing," *IEEE Photon. Technol. Lett.*, vol. 13, pp. 1292-1294, Dec. 2001.
- [11] W. C. H. Choy, "Optical properties of InGaAs/InAlAs diffused double quantum wells," *J. Appl. Phys.*, vol. 87, pp. 2956-2966, 2000.
- [12] A. T. Meney, "Exciton binding energies and absorption in intermixed GaAs/AlGaAs quantum well," *J. Appl. Phys.*, vol. 71, pp. 5729-5734, 1992.
- [13] S. Tomić, Z. Ikončić, and V. Milanovic, "Interdiffusion-based optimal quantum-well profile shaping for unipolar quantum-fountain lasers," *J. Appl. Phys.*, vol. 91, pp. 4801-4805, 2002.
- [14] W. C. H. Choy, "Tailoring light- and heavy-holes of GaAsP/AlGaAs quantum wells by using interdiffusion for polarization independent amplifier applications," *IEEE J. Quantum Electron.*, vol. 36, pp. 164-174, Feb. 2000.
- [15] K. S. Chan, E. H. Li, and M. C. Y. Chan, "Optical gain of interdiffused InGaAs-GaAs and AlGaAs-GaAs quantum wells," *IEEE J. Quantum Electron.*, vol. 34, pp. 157-165, Jan. 1998.
- [16] E. H. Li, "Refractive index of interdiffused AlGaAs/GaAs quantum well," *J. Appl. Phys.*, vol. 82, pp. 6251-6258, 1997.
- [17] S. F. Yu and E. H. Li, "Proposed enhancement of side mode suppression ratio in  $\lambda/4$  shifted distributed feedback lasers with nonuniform diffused quantum wells," *IEEE Photon Technol. Lett.*, vol. 8, pp. 482-484, Apr. 1996.
- [18] S. F. Yu, C. W. Lo, and E. H. Li, "Investigation of high power single mode operation in DFB and FP lasers using diffused quantum well structures," *IEEE J. Quantum Electron.*, vol. 33, pp. 999-1009, 1997.
- [19] M. Ghisoni, P. J. Stevens, G. Parry, and J. S. Roberts, "Post-growth tailoring of the optical properties of GaAs/AlGaAs quantum well structures," *Opt. Quantum Electron.*, vol. 23, pp. S915-S924, 1991.
- [20] J. Micallef, E. H. Li, and B. L. Weiss, "Effects of interdiffusion on the sub-band-edge structure of  $\text{In}_{0.53}\text{Ga}_{0.47}\text{As}/\text{InP}$  single quantum wells," *J. Appl. Phys.*, vol. 73, pp. 7524-7532, 1993.
- [21] T. K. Sodoh, M. Kumano, Y. Nokano, and K. Tada, "Wavelength trimming by photoabsorption-induced disordering for multiple-wavelength distributed-feedback laser arrays," *IEEE Photon. Technol. Lett.*, vol. 9, pp. 887-888, 1997.
- [22] K. S. Chan, L. Zhan, and E. Y. B. Pun, "Theoretical analysis of wavelength tuning in distributed feedback lasers by quantum well intermixing," *IEEE Photon. Technol. Lett.*, vol. 13, pp. 1058-1060, Oct. 2001.
- [23] L. Zhan, K. S. Chan, E. Y. B. Pun, and H. P. Ho, "Wavelength shift enhancement in quantum-well intermixed distributed-feedback lasers," *IEEE Photon. Technol. Lett.*, vol. 14, pp. 744-746, June 2002.
- [24] S. L. Chuang, *Physics of Optoelectronic Devices*. New York: Wiley, 1995, ch. 10.
- [25] T. Yamaguchi, T. Morimoto, K. Akeura, K. Tada, and Y. Nakano, "Polarization-independent waveguide modulator using a novel quantum well with mass-dependent width," *IEEE Photon. Technol. Lett.*, vol. 6, pp. 1442-1442, Dec. 1994.
- [26] W. C. H. Choy and E. H. Li, "Polarization insensitive optical modulation in a diffused parabolic-like quantum well," *Appl. Opt.*, vol. 37, pp. 1674-1681, 1998.
- [27] E. S. Koteles, F. Agahi, K. M. Lau, A. Baliga, and N. G. Anderson, "Quantum well structures with almost degenerate valence bands," *Proc. SPIE*, vol. 2139, pp. 103-114, 1994.
- [28] W. C. H. Choy, H. Feng, S. K. Kam, and E. H. Li, "The effect of composition modification on the optical polarization independence in semiconductor strain quantum wells," in *Proc. Mat. Res. Soc. Symp.*, vol. 417, 1996, pp. 277-282.
- [29] S. L. Ng, H. S. Lim, Y. L. Lam, Y. C. Chan, B. S. Ooi, V. Aimez, J. Beauvais, and J. Beerens, "Polarization insensitive InGaAs/InGaAsP electro-absorption intensity modulator using quantum well intermixing process," *Electron. Lett.*, vol. 38, pp. 241-242, 2002.
- [30] W. C. H. Choy, E. H. Li, and J. Micallef, "The polarization insensitive electro-absorptive and -refractive modulation by utilizing InGaAsP/InP interdiffused quantum well," *IEEE J. Quantum Electron.*, vol. 33, pp. 1316-1322, 1997.

**Wallace C. H. Choy** received the B.Sc. (first class honors) degree in applied physics from the Baptist University of Hong Kong, Kowloon, Hong Kong, the M.Phil. degree in electronic engineering from the University of Hong Kong, Hong Kong, and the Ph.D. degree in electronic engineering from the University of Surrey, Surrey, U.K., in 1999. His postgraduate research was involved in modeling of optical properties of quantum wells and interdiffusion modified quantum-well structures for acoustooptical and electrooptical modulators.

He joined the National Research Council (NRC) of Canada in 1999 as a Member of Research Staff where he worked, both theoretically and experimentally, on the projects of InP-based polarization-independent optical amplifiers and switches. He was also involved in investigating Si-based MUX/DEMUX devices. He joined Fujitsu Compound Semiconductor Inc., San Jose, CA, in 2001 to develop tunable laser and high-speed transmitter modules. Since 2003, he has been with the Department of Electrical and Electronic Engineering, University of Hong Kong. His current research interests are concerned with quantum-well intermixing, nanotechnology, and optical transmitter modules. He also broadens his interest in organic LED. Since 1994, he has published more than 35 international technical papers and contributed to a book chapter.

Dr. Choy was awarded the Sir Edward Youde Memorial Fellowship, Postgraduate Studentship award, first prize of the 1996 IEEE HK section PGS paper competition while performing his graduate work in Hong Kong, and a Croucher Foundation Scholarship during his research work at Surrey. He received the Outstanding Achievement Award from NRC in 2001.

**K. S. Chan** received the B.Sc. (first class honors) and Ph.D. degrees in physics from the University of Hong Kong, Hong Kong.

He was a Research Fellow at the University of Oxford, Oxford, U.K., for two years, where he started his study of low-dimensional semiconductor structure under the supervision of Prof. R. J. Elliott. He then worked in the semiconductor research group at the University of Nottingham, Nottingham, U.K., for two years before he joined City University of Hong Kong (City U), Kowloon, Hong Kong, where he is currently an Associate Professor. He was the Associate Head of the Department of Physics and Materials Science at City U from 2000 to 2003. He was the Council Chairman of the Hong Kong Physical Society and Vice-Chairman of the SPIE Hong Kong Chapter. He was an adviser to Maxford Technology, an industrial company specialized in thin film technology, and a consultant to CN Electronics on photonics. His research interests are particularly concerned with the physics of low-dimensional semiconductor structures, nanotechnology, quantum-well intermixing, and the modeling of semiconductor optoelectronic devices. He has published two book chapters and more than 60 journal and conference papers.